Electronic Supplementary Material (ESI) for Physical Chemistry Chemical Physics.
This journal is © the Owner Societies 2020

New structural model of a chiral cubic liquid crystalline phase

Nataša Vaupotič, Mirosław Salamończyk, Joanna Matraszek, Martin Vogrin, Damian Pociecha, Ewa Gorecka

Modelling of the XRD response

The electron density $\rho(\vec{r})$ map is reconstructed from the amplitudes of the form factors ($|F_{hkl}|$) and their phases (ϕ_{hkl}) as

$$\rho(\vec{r}) = \sum_{h,k,l} |F_{hkl}| \cos\left(\vec{q} \cdot \vec{r} + \phi_{hkl}\right)$$

where $\vec{q}$ is a scattering vector. The highest intensity peaks recorded for the CC phase are the peaks with Miller indices (004), (123), (420) and (222). For structures with a centre of inversion (such as the $Im\bar{3}m$ symmetry) the phase ϕ_{hkl} can be only 0 or π; however, for a chiral cubic phase with no centre of inversion the peak (123) can have any phase between 0 and π. All the possibilities of combination of phases have already been studied in details and the corresponding density maps are given in [1]. It was shown that the electron density maps reconstructed with a general phase of the (123) peak are closely related to the electron density maps obtained for the $Im\bar{3}m$ symmetry structure. Intermediate values of ϕ_{123} introduce different degrees of distortion which are not physically plausible. Here we show the electron density maps (**Supplementary Figure 1**) only for the phases given in **Supplementary Table 1**, at a density cut off such that 1/3 of the unit cell volume is within the shaded region (this is approximately the volume occupied by aromatic cores) and at a higher density cut-off, such that 1/6 of the unit cell with the highest density is shaded.

Supplementary Table 1. Magnitudes of the form factors $|F_{hkl}|$ for the peaks with Miller indices (hkl) and the corresponding phases (ϕ_{hkl}) used for the reconstruction of the electron density maps [2,3]. The form factors are calculated as $\sqrt{I_{hkl}/M}$, where the intensities of the peaks (I_{hkl}) and their multiplicity (M) are given in **Table 3** of the main paper.

(hkl)	$\lvert F_{hkl}\rvert$	ϕ_{hkl}
(004)	1	$0^{[2]}\ or\ \pi^{[3]}$
(123)	0.69	π
(024)	0.24	0
(222)	0.41	0

The obtained electron density maps show that the structure with micelles in the centre and edges of the unit cell (obtained for $\phi_{004} = \pi$) has a more uniform electron density of the middle grid. In addition, in case of $\phi_{004} = 0$, the connections among the hexagons are much denser that the connections within each hexagon, as can be seen from the electron density map in **Supplementary Figure 1.**

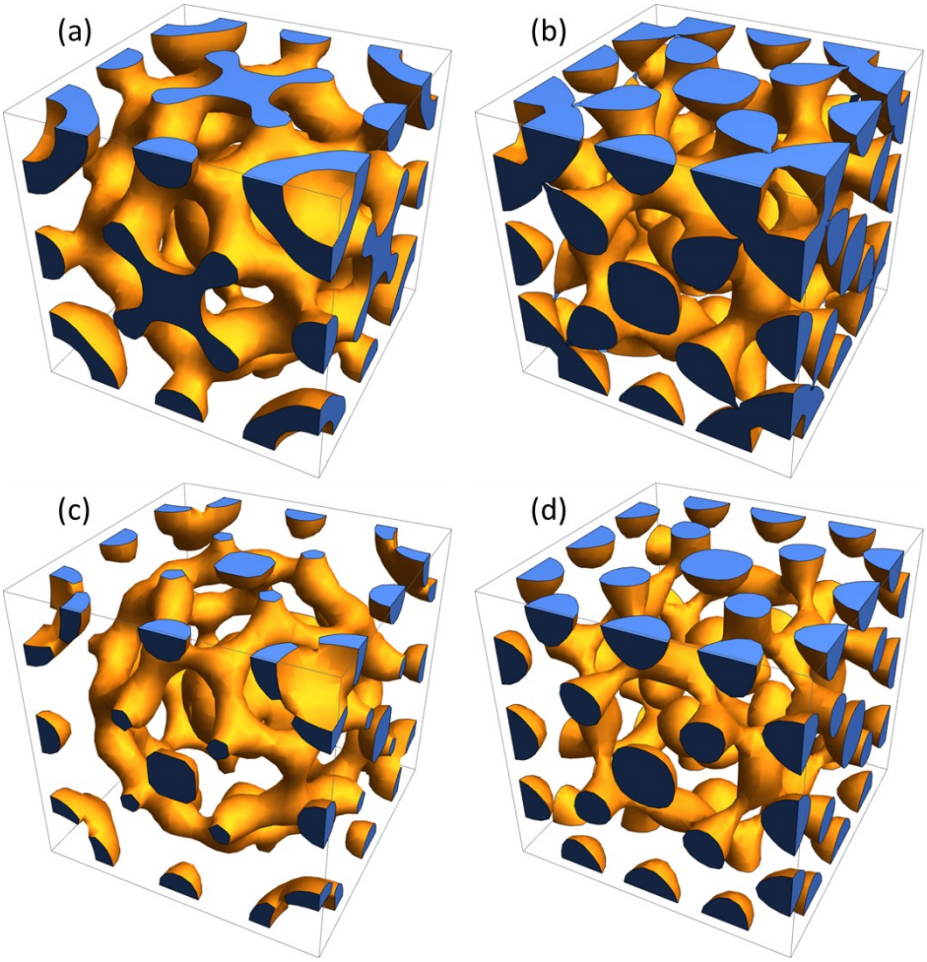

Supplementary Figure 1. Electron density maps of the CC phase obtained with the form factors given in **Supplementary Table 1** at lower (a) and (b) and higher (c) and (d) cut-offs. The shaded volume at lower cut-off is approximately 1/3 of the unit cell and 1/6 at the higher cut-off. In (a) and (c) the phase of the (004) peak is π and in (b) and (d) it is 0.

As explained in the main text, two models for the middle grid (Supplementary Table 2) were used to theoretically predict the intensities of the peaks detected in XRD measurements of the CC phase. Both models give almost planar 3-fold junctions of channels (in the $Ia\bar{3}d$ phase junctions are planar); however, model 2 gives the length (l) of the segments within the hexagons almost equal to the length of the channels in the $Ia\bar{3}d$ phase (by taking the cell parameter in the CC being 50% larger than in the $Ia\bar{3}d$ phase, $l = 0.34\ a_{DG}$ in the CC phase and $l = 0.35\ a_{DG}$ in the $Ia\bar{3}d$ phase, where a_{DG} is the unit cell length in the $Ia\bar{3}d$ phase), while in case of model 1, the length of channels within the hexagons is $l = 0.27\ a_{DG}$, i.e. much lower than in the $Ia\bar{3}d$ phase.

Supplementary Table 2. The positions of generating points (in units of the unit cell parameter of the chiral cubic phase a_{CC}), lengths of the hexagon side (l) and the angle between the neighboring segments (γ) for the two models considered for the calculation of the XRD response.

	Generating point	l/a_{CC}	$\gamma\ [deg]$
Model 1	$(0.181, 0.181, 0.407)$	0.181	118.5
Model 2	$(0.151, 0.151, 0.425)$	0.226	118.6

In the calculation of the XRD response we proceeded as follows. Micelles of a radius r_m and thickness Δr_m are placed in the corners of the unit cell and in its centre. The form factor of a micelle is obtained from a form factor of a spherical shell (F_{shell}) with radius r [4]:

$$F_{shell} = \frac{\sin(qr)}{qr} \quad .$$

Summing up the contributions from a shell with a radius from $r_m - \Delta r_m/2$ to $r_m + \Delta r_m/2$, one finds the form factor of a micelle (F_m) [4,5]:

$$F_m = \frac{4\pi}{q^3}\left[f\left(q\left(r_m + \frac{\Delta r_m}{2}\right)\right) - f\left(q\left(r_m - \frac{\Delta r_m}{2}\right)\right)\right] \quad ,$$

where

$$f\left(q\left(r_m \pm \frac{\Delta r_m}{2}\right)\right) = \sin\left[q\left(r_m \pm \frac{\Delta r_m}{2}\right)\right] - q\left(r_m \pm \frac{\Delta r_m}{2}\right)\cos\left[q\left(r_m \pm \frac{\Delta r_m}{2}\right)\right] \quad .$$

In the middle grid, channels are modelled by cylinders, their length being given by the distance between the junctions. The form factor of one cylinder (F_c) with its long axis at an angle α with respect to the direction of the wave vector $\vec{q}$ is [4,5]:

$$F_c = 2\pi R^2 L \frac{\sin\left(q\frac{L}{2}\cos\alpha\right) J_1(qR\sin\alpha)}{q\frac{L}{2}\cos\alpha \qquad qR\sin\alpha} \quad ,$$

where R and L are the radius and length of the cylinder, respectively. The structure factor (F) is a sum of form factors including the phase due to the position of the micelle or cylinder:

$$F = \rho_m \sum_j F_m^{(j)} e^{i\vec{q}\cdot\vec{r}_j} + \rho_{ch} \sum_j F_c^{(j)} e^{i\vec{q}\cdot\vec{r}_j} + \rho_{cc} \sum_j F_c^{(j)} e^{i\vec{q}\cdot\vec{r}_j} \quad ,$$

where ρ_m is a density of micelles and ρ_{ch} and ρ_{cc} the density of the cylinders forming the hexagons and the ones connecting either the hexagons (Model 1) or connecting hexagons to the edges and faces of the unit cell (Model 2), respectively. The sums are taken over all the micelles and cylinders in the unit cell and $\vec{r}_j$ is a position of the centre of a chosen micelle or cylinder.

As explained in the main text, the densities of the micelles and the cylinders forming the hexagons, as well as the cylinders connecting the hexagons are assumed to be equal. The density of the cylinders connecting the hexagon apexes with the edges or faces of the unit cell is lower. There are thus three fitting parameters (r_m, Δr_m, r_c) for Model 1 and four fitting parameters (r_m, Δr_m, r_c, ρ_{cc}) for Model 2. The results are given in the main text. Here we add, that by considering the electron density maps for the structure with micelles (**Supplementary Figure 1**) one can see, that there seem to be connections both among the hexagons as well as from the hexagons to the centres of edges and faces of the unit cell and that the latter are of lower density. Thus, we modelled the XRD response also by taking the generating point of Model 1 and replaced the connections between the neighbouring hexagons by the connections from the hexagons to the unit cell edges and centres. No match between theory and experiment was found. Next, we used the generating point of Model 2 and replaced the connections to the cube faces and edges by the connections among hexagons. In this case, a match was found (see **Supplementary Table 3**), but not as good as for the original Model 2.

Supplementary Table 3. Experimental intensities ($I_{hkl}^{(exp)}$) of the peaks with Miller indices (hkl), multiplicity of the peaks (M) and the intensities (I_{C1} and I_{C2}) obtained for the generating point $(0.151,0.151,0.425)a_{CC}$; Case 1: connections among hexagons; $r_m = 0.212a_{CC}$, $dr_m = 0.045a_{CC}$, $r_c = 0.06a_{CC}$; Case 2: connections to the cube edges and faces; $r_m = 0.22a_{CC}$, $dr_m = 0.05a_{CC}$, $r_c = 0.075a_{CC}$, $\rho_{cc}/\rho_m = 0.3$.

(hkl)	M	$I_{hkl}^{(exp)}$	I_{C1}	I_{C2}
011	12		0	0.03
002	6		0.04	0.03
112	24	0.002	0.25	0.06
022	12	0.001	0.14	0.02
013	24	0.007	0.01	0.06
222	8	0.057	0.02	0.001
123	48	1	1	1
004	6	0.26	0.33	0.25
114	24	0.03	0.11	0.004
033	12			
024	24	0.06	0.01	0.16
233	24		0.05	0.04
224	24	0.005	0.05	0.08

Modelling of the elastic energy

The Helfrich energy (μ_C) of the iso-electron-density surfaces is defined as

$$\mu_C = \int_S \left(\frac{1}{2}\kappa_H (H - H_0)^2 + \kappa_G K\right) dS$$

where H and K are the mean and the Gaussian curvature, respectively, and κ_H and κ_G are the corresponding moduli. In a series of experiments [6-9], it was observed that $\kappa_G \simeq -\kappa_H$, but as shown in **Supplementary Figure 2**, the ratio between the magnitudes does not play a role in our conclusions. By H_0 we denote the natural curvature of the assemblies, which is zero for the studied system. The Helfrich energy was calculated for different volume ratios (V_r) enclosed by the iso-electron-density surface (**Supplementary Table 4**). We see that the Helfrich energy is systematically lower for the CC phase reconstructed by the phases of the (123) and (004) peaks being both π. In calculation of the energy of the $Ia\bar{3}d$ phase the volume of the $Ia\bar{3}d$ phase was chosen to be equal to the volume of one unit cell in the CC phase. By considering the experimental values for a_{DG}/a_{CC} being approximately $2/3$ we took a cube with a side equal to $1.5a_{DG}$ for calculating the energy of the $Ia\bar{3}d$ phase. We also repeated the calculations by taking $a_{CC} = 1.6a_{DG}$ (the values at the temperature for which the XRD data in the main paper, **Figure 4**, is given). Finally, we calculated the Helfrich energy for the recently proposed model with the $I23$ symmetry [10]. At the volume ratio enclosed by the iso-electron-density-surface being 0.33 and the side of the unit cell in the chiral cubic phase being 1.6-times larger than in the double gyroid phase, the ratio between the Helfrich energy in the chiral cubic and double gyroid phase is 2.9.

Supplementary Table 4. The Gaussian curvature (K), the variance of the mean curvature ($\frac{1}{2}(H-H_0)^2$) and the Helfich energy (μ_C), assuming $\kappa_K = -\kappa_H$ for the iso-electron-density surfaces of CC and $Ia\bar{3}d$ phases. The energy of the CC phase is calculated with the phases of the (123) and (004) peaks being both π ($CC_{(\pi,\pi)}$) and with the phase of the (004) peak being 0 ($CC_{(\pi,0)}$). Different volume ratios (V_r) enclosed by the iso-electron-density surfaces were considered. In the last column the ratio between the Helfrich energy of the CC and $Ia\bar{3}d$ phase is collected, at the same volume ratio. The size of the unit cell in the CC was taken as 1.5 and 1.6 times the size of the $Ia\bar{3}d$ unit cell, the latter values being given in the parenthesis.

Phase	V_r	K [au]	$\frac{1}{2}(H-H_0)^2$ [au]	μ_C [au]	$\mu_C^{(CC)}/\mu_C^{(Ia\bar{3}d)}$
$CC_{(\pi,0)}$	0.30	-886	171	1057	2.5 (2.1)
	0.33	-882	128	1010	2.5 (2.1)
	0.36	-922	105	1027	2.6 (2.2)
$CC_{(\pi,\pi)}$	0.30	-467	182	649	1.5 (1.3)
	0.33	-486	182	668	1.6 (1.4)
	0.36	-477	190	667	1.7 (1.4)
$Ia3d$	0.30	-352 (-422)	68 (81)	420 (503)	
	0.33	-350 (-420)	57 (68)	407 (488)	
	0.36	-348 (-418)	47 (58)	395 (476)	

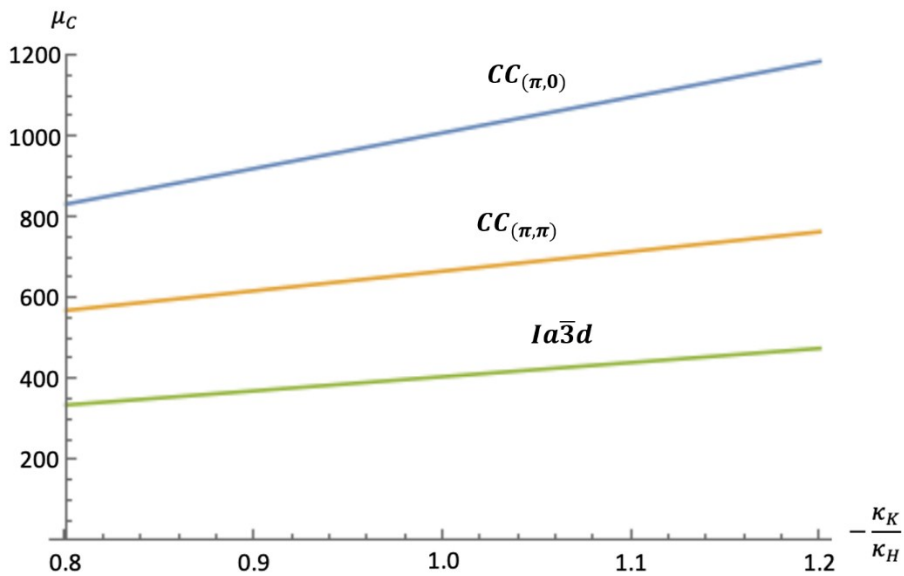

Supplementary Figure 2. The Helfrich energy (μ_C) as a function of ratio between the mean (κ_H) and the Gaussian (κ_G) curvature moduli for the $Ia\bar{3}d$ and CC phase calculated with phases of the (123) and (004) being both π (

$CC_{(\pi,\pi)}$) and with the phase of the (004) peak being 0 ($CC_{(\pi,0)}$). The size of the unit cell in the CC was taken as 1.5 the size of the $Ia\bar{3}d$ unit cell.

Supplementary References

[1] X. Zeng, L. Cseh, G. H. Mehl, G. Ungar, *J. Mater. Chem.,* 2008, **18**, 2953-2961.

[2] K. Ozawa, Y. Yamamura, S. Yasuzuka, H. Mori, S. Kutsumizu, K. Saito, *J Phys Chem B,* 2008, **112**, 12179-81.

[3] X. Zeng, G. Ungar, M. Impéror-Clerc, *Nat. Mater.,* 2005, **4**, 562–567.

[4] J. S. Pedersen, *Adv. Colloid Interface Sci.,* 1997, **70**, 171-210.

[5] GISAXS Community website http://gisaxs.com/index.php/Form_Factor

[6] R. H. Templer, J. M. Seddon, N. A. Warrender, A. Syrykh, Z. Huang, R. Winter, J. Erbes, *J. Phys. Chem. B,* 1998, **102**, 7251-7261.

[7] R. H. Templer, B. J. Khoo, J. M. Seddon, *Langmuir,* 1998, **14**, 7427-7434.

[8] H. Vacklin, B. J. Khoo, K. H. Madan, J. M. Seddon, R. H. Templer, *Langmuir,* 2000, **16**, 4741-4748.

[9] J. Zimmerberg, M. M. Kozlov, *Nat. Rev. Mol. Cell. Biol.,* 2006, **7**, 9-19.

[10] X. Zeng and G. Ungar, *J. Mater. Chem. C*, 2020, **8**, 5389-5398.